

**NEUTRINO SCATTERING IN STRANGENESS-RICH STELLAR MATTER**

SANJAY REDDY AND MADAPPA PRAKASH

Physics Department  
State University of New York at Stony Brook  
Stony Brook, NY 11794-3800, USA**ABSTRACT**

We calculate neutrino cross sections from neutral current reactions in dense matter containing hyperons. We show that  $\Sigma^-$  hyperons give significant contributions. To lowest order, the contributions from the neutral  $\Lambda$  and  $\Sigma^0$ , which have zero hypercharge, vanish. However, their presence furnishes baryon number which decreases the relative concentrations of nucleons. This leads to significant reductions in the cross sections. Due to the uncertainty in strong interactions at high density, the neutrino opacity may vary by a factor of about 2 depending on the behavior of the effective masses.

*Subject headings:* dense matter – stars: neutron – stars: opacities – stars: neutrinos

**1 Introduction**

The general nature of the neutrino signature expected from a newly formed neutron star (hereafter referred to as a protoneutron star) has been theoretically predicted (Burrows & Lattimer 1986) and confirmed by the observations (Bionta et al. 1987; Hirata et al 1987) from supernova SN1987A. Although neutrinos interact weakly with matter, the high baryon densities and neutrino energies achieved after the gravitational collapse of a massive star ( $\geq 8$  solar masses) cause the neutrinos to become trapped on the dynamical timescales of collapse (Sato 1975; Mazurek 1975). Trapped neutrinos at the star's core have Fermi energies  $E_\nu \sim 200 - 300$  MeV and are primarily of the  $\nu_e$  type. They escape after diffusing through the star exchanging energy with the ambient matter, which has an entropy per baryon of order unity in units of Boltzmann's constant. Eventually they emerge from the star with an average energy  $\sim 10 - 20$  MeV and in nearly equal abundance of all three flavors, both particle and anti-particle.

Neutrino interactions in dense matter have been investigated by various authors (Tubbs & Schramm 1975; Sawyer 1975,89,95; Lamb & Pethick 1976; Lamb 1978; Sawyer & Soni

1979; Iwamoto & Pethick 1982; Iwamoto 1982; Goodwin & Pethick 1982; Burrows & Mazurek 1982; Bruenn 1985; van den Horn & Cooperstein 1986; Cooperstein 1988; Burrows 1988; Horowitz & Wehrberger 1991a,b;1992; Reddy & Prakash 1995). The charged current absorption and neutral current scattering reactions are both important sources of opacity. The neutral current scattering involves all flavors of neutrinos scattering on nucleons and leptons. Scattering from electrons is important for energy and momentum transfer (Tubbs & Schramm, 1975). The influence of interactions for neutrino-electron scattering is also important (Horowitz 1992) and increases the mean free path by 50-60% for electron type neutrinos. However, for lepton number transport, nucleon scattering and absorption are the dominant processes.

Surprisingly little attention has been paid to the effects of composition and of strong interactions of the ambient matter on neutrino opacities. The effect of interactions was investigated for non-degenerate nuclear matter by Sawyer (1975; 1989) and for degenerate pure neutron matter by Iwamoto & Pethick (1982). Treating nucleons in the non-relativistic limit, these calculations predict an increase in the mean free path by a factor of  $\sim 2 - 3$ , for (2-4) times the nuclear density. More recently, relativistic calculations based on effective Lagrangian models for dense neutron star matter have been performed by Horowitz & Wehrberger (1991a,b;1992). Here, the differential cross sections for matter containing nucleons and electrons were calculated using linear response theory. A reduction of 30-50% over the case of non-interacting nucleons was reported in these calculations. The influence of interactions has been investigated in protoneutron star calculations only by a simple scaling of the non-interacting results (Burrows 1990, Keil 1994). Furthermore, there have been no calculations performed including the multi-component nature of the system. We note that Keil & Janka (1995) have recently carried out cooling simulations including hyperons in the equation of state (EOS), but they ignored opacity modifications. We view it as essential that opacities be consistent with the composition, which has not been a feature of protoneutron star models to date.

Although the composition and EOS of the hot protoneutron star matter are not yet known with certainty, QCD based effective Lagrangians have opened up intriguing possibilities (Kaplan & Nelson 1986; Glendenning 1986,1992; Glendenning & Moszkowski 1991; Kapusta & Olive 1990; Ellis, Knorren & Prakash 1995; Knorren, Prakash & Ellis 1995, Prakash, Cooke & Lattimer 1995). Among these is the possible existence of matter with strangeness to baryon ratio of order unity. Strangeness may be present either in the form of fermions, notably the  $\Lambda$  and  $\Sigma^-$  hyperons, or, in the form of a Bose condensate, such as a  $K^-$ - meson condensate, or, in the form of  $s$  quarks. In the absence of trapped neutrinos, strange particles are expected to appear around 2 – 4 times the nuclear matter density of  $n_0 = 0.16 \text{ fm}^{-3}$ . Neutrino-trapping causes the strange particles to appear at somewhat higher densities, since the relevant chemical potential  $\mu = \mu_e - \mu_{\nu_e}$  in matter with high lepton content is much smaller than in the untrapped case (Ellis, Knorren & Prakash 1995; Knorren, Prakash & Ellis 1995).

A new feature that we consider here is the role of strangeness. To date, only neutrino opacities for strange quark matter have been calculated (Iwamoto, 1982). Here, we study neutrino mean free paths in matter containing strangeness in the form of hyperons. Specifically, we calculate neutrino opacities from neutral current reactions in matter containing hyperons and which are faithful to the EOS. In a first effort, this will be achieved using a

mean field theoretical description which includes hyperonic degrees of freedom. This approach has several merits. For example, aspects of relativity, which may become important at high density, are naturally incorporated. Modifications of the opacity due to correlations (RPA) are also possible in such an approach. Further, comparisons with alternative potential model approaches (Iwamoto & Pethick 1982; Sawyer 1989) are straightforward. Neutrino opacities in matter containing other forms of strangeness and from charged current reactions (Prakash et. al. 1992) will be considered in a separate work.

In §2, neutrino interactions with strange baryons are discussed. In §3, the composition of beta-equilibrated matter with strange baryons is determined based on a field theoretic description. §4 contains our results along with discussion. Conclusions are given in §5.

## 2 Neutrino Interactions with Strange Baryons

Neutrino interactions with matter proceed via charged and neutral current reactions. The neutral current processes contribute to elastic scattering, and charged current reactions result in neutrino absorption. The formalism to calculate neutral current scattering rates in dense matter is summarized below. The interaction Lagrangian for neutrino scattering reactions is given by the Wienberg-Salam theory:

$$\mathcal{L}_{int}^{nc} = (G_F/2\sqrt{2}) l_\mu j_z^\mu \quad \text{for} \quad \nu + B \rightarrow \nu + B, \quad (1)$$

where  $G_F \simeq 1.436 \times 10^{-49}$  erg cm<sup>-3</sup> is the weak coupling constant. The neutrino and target particle weak neutral currents appearing above are:

$$\begin{aligned} l_\mu^\nu &= \bar{\psi}_\nu \gamma_\mu (1 - \gamma_5) \psi_\nu \\ j_z^\mu &= \bar{\psi}_i \gamma^\mu (C_{Vi} - C_{Ai} \gamma_5) \psi_i, \end{aligned} \quad (2)$$

where  $i = n, p, \Lambda, \Sigma^-, \Sigma^+, \Sigma^0, \Xi^-, \dots$  and  $e^-, \mu^-$ . The neutral current process couples neutrinos of all types ( $e, \mu$  and  $\tau$ ) to the weak neutral hadronic current,  $j_z^\mu$ . The vector and axial vector coupling constants,  $C_{Vi}$  and  $C_{Ai}$ , are listed in Table 1. Numerical values of the parameters that best fit data on charged current semi-leptonic decays of hyperons are (Gaillard & Sauvage 1984):  $D=0.756$ ,  $F=0.477$ ,  $\sin^2 \theta_W=0.23$  and  $\sin \theta_c = 0.231$ . Tree level coupling of neutrinos to the neutral particles  $\Lambda$  and  $\Sigma^0$  vanish, since the Z boson couples to the hyper-charge, which is zero for both the  $\Lambda$  and  $\Sigma^0$ . Neutrino scattering off leptons in the same family involves charged current couplings as well, and one has to sum over both the contributing diagrams. At tree level, however, one can express the total coupling by means of a Fierz transformation; this is accounted for in Table 1.

Given the general structure of the neutrino coupling to matter, the differential cross section for elastic scattering for incoming neutrino energy  $E_\nu$  and outgoing neutrino energy  $E'_\nu$  is given by

$$\frac{1}{V} \frac{d^3\sigma}{d\Omega'^2 dE'_\nu} = -\frac{G^2}{128\pi^2} \frac{E'_\nu}{E_\nu} \text{Im} (L_{\alpha\beta} \Pi^{\alpha\beta}), \quad (3)$$

where the neutrino tensor  $L_{\alpha\beta}$  and the target particle polarization  $\Pi^{\alpha\beta}$  are

$$L_{\alpha\beta} = 8[2k_\alpha k_\beta + (k \cdot q)g_{\alpha\beta} - (k_\alpha q_\beta + q_\alpha k_\beta) \mp i\epsilon_{\alpha\beta\mu\nu} k^\mu q^\nu] \quad (4)$$

TABLE 1

## NEUTRAL CURRENT VECTOR AND AXIAL COUPLINGS

Reaction	$C_V$	$C_A$
$\nu_e + e \rightarrow \nu_e + e$	$1 + 4 \sin^2 \theta_W = 1.92$	1
$\nu_e + \mu \rightarrow \nu_e + \mu$	$-1 + 4 \sin^2 \theta_W = -0.08$	-1
$\nu_i + n \rightarrow \nu_i + n$	-1	$-D - F = -1.23$
$\nu_i + p \rightarrow \nu_i + p$	$1 - 4 \sin^2 \theta_W = 0.08$	$D + F = 1.23$
$\nu_i + \Lambda \rightarrow \nu_i + \Lambda$	0	0
$\nu_i + \Sigma^- \rightarrow \nu_i + \Sigma^-$	$-2 + 4 \sin^2 \theta_W = -1.08$	$-2F = -0.95$
$\nu_i + \Sigma^+ \rightarrow \nu_i + \Sigma^+$	$2 - 4 \sin^2 \theta_W = 1.08$	$2F = 0.95$
$\nu_i + \Sigma^0 \rightarrow \nu_i + \Sigma^0$	0	0
$\nu_i + \Xi^- \rightarrow \nu_i + \Xi^-$	$-1 + 4 \sin^2 \theta_W = -0.08$	$D = 0.756$
$\nu_i + \Xi^0 \rightarrow \nu_i + \Xi^0$	1	$-D + F = -0.28$

NOTE.— Coupling constants derived assuming SU(3) symmetry for the hadrons. Numerical values are quoted using  $D=0.756$ ,  $F=0.477$ ,  $\sin^2 \theta_W=0.23$  and  $\sin \theta_c = 0.231$  (Gaillard & Sauvage 1984). At tree level, the  $\Lambda$  and  $\Sigma^0$ , which have zero weak-hypercharge, do not couple to the neutrinos.

$$\Pi_{\alpha\beta}^i = -i \int \frac{d^4 p}{(2\pi)^4} \text{Tr} [G^i(p) J_\alpha G^i(p+q) J_\beta]. \quad (5)$$

Above,  $k_\mu$  is the incoming neutrino four momentum, and  $q_\mu$  is the four momentum transfer. The Greens' functions  $G^i(p)$  (the index  $i$  labels particle species) depend on the Fermi momentum  $k_{Fi}$  of target particles. In the Hartree approximation, the propagators are obtained by replacing  $M_i$  and  $k_{Fi}$  in the free particle propagators by  $M_i^*$  and  $k_{Fi}^*$  (see below), respectively. The current operator  $J_\mu$  is  $\gamma_\mu$  for the vector current and  $\gamma_\mu \gamma_5$  for the axial current. Given the V–A structure of the particle currents, we have

$$\Pi_{\alpha\beta}^i = C_{Vi}^2 \Pi_{\alpha\beta}^{Vi} + C_{Ai}^2 \Pi_{\alpha\beta}^{Ai} - 2C_{Vi} C_{Ai} \Pi_{\alpha\beta}^{VAi}. \quad (6)$$

For the vector polarization,  $\{J_\alpha, J_\beta\} :: \{\gamma_\alpha, \gamma_\beta\}$ , for the axial polarization,  $\{J_\alpha, J_\beta\} :: \{\gamma_\alpha \gamma_5, \gamma_\beta \gamma_5\}$  and for the mixed part,  $\{J_\alpha, J_\beta\} :: \{\gamma_\alpha \gamma_5, \gamma_\beta\}$ . Further, the polarizations contain two parts: the density dependent part that describes particle-hole excitations and the Feynman part that describes particle-antiparticle excitations. For elastic scattering, with  $q_\mu^2 < 0$ , the contribution of the Feynman parts vanish. Using vector current conservation and translational invariance,  $\Pi_{\alpha\beta}^V$  may be written in terms of two independent components. In a frame where  $q_\mu = (q_0, |q|, 0, 0)$ , we have

$$\Pi_T = \Pi_{22}^V \quad \text{and} \quad \Pi_L = -\frac{q_\mu^2}{|q|^2} \Pi_{00}^V.$$

The axial current-current correlation function can be written as a vector piece plus a cor-

rection term:

$$\Pi_{\mu\nu}^A = \Pi_{\mu\nu}^V + g_{\mu\nu}\Pi^A. \quad (7)$$

The mixed, axial current-vector current correlation function is

$$\Pi_{\mu\nu}^{VA} = i\epsilon_{\mu,\nu,\alpha,0}q^\alpha\Pi^{VA}. \quad (8)$$

The above mean field or Hartree polarizations, which characterize the response of the medium to the neutrino, have been explicitly evaluated in previous work (Horowitz & Wehrberger 1991). In terms of these polarizations, the differential cross section is

$$\frac{1}{V} \frac{d^3\sigma}{d\Omega'^2 dE'_\nu} = -\frac{G^2}{16\pi^3} \frac{E'_\nu}{E_\nu} q_\mu^2 [AR_1 + R_2 + BR_3], \quad (9)$$

with

$$A = \frac{2k_0(k_0 - q_0) + q_\mu^2/2}{|q|^2} \quad ; \quad B = 2k_0 - q_0. \quad (10)$$

The polarizations may be combined into three uncorrelated response functions,  $R_1$ ,  $R_2$  and  $R_3$ , by summing over the contributions from each particle species  $i$ :

$$R_1 = \sum_i [C_{V_i}^2 + C_{A_i}^2][Im(\Pi_T^i) + Im(\Pi_L^i)], \quad (11)$$

$$R_2 = \sum_i C_{V_i}^2[Im(\Pi_T^i)] + C_{A_i}^2[Im(\Pi_T^i) - Im(\Pi_A^i)], \quad (12)$$

$$R_3 = \pm \sum_i 2C_{A_i}C_{A_i} Im(\Pi_{VA}^i). \quad (13)$$

These functions depend upon the the individual  $k_{Fi}$  (or the concentration) and the corresponding effective masses  $M_i^*$ , for which a many-body description of the multi-component system is required.

### 3 Composition of Matter with Strange Baryons

To explore the influence of the presence of hyperons in dense matter, we employ a relativistic field theoretical model in which the interactions between baryons are mediated by the exchange of  $\sigma$ ,  $\omega$  and  $\rho$  mesons. The full Lagrangian density is given by (Serot & Walecka 1986),

$$\begin{aligned} L = & \sum_B \bar{B}(-i\gamma^\mu\partial_\mu - g_{\omega B}\gamma^\mu - g_{\rho B}\gamma^\mu\mathbf{b}_\mu \cdot \mathbf{t} - M_B + g_{\sigma B}\sigma)B \\ & - \frac{1}{4}W_{\mu\nu}W^{\mu\nu} + \frac{1}{2}m_\omega^2\omega_\mu\omega^\mu - \frac{1}{4}\mathbf{B}_{\mu\nu}\mathbf{B}^{\mu\nu} + \frac{1}{2}m_\rho^2\rho_\mu\rho^\mu \\ & + \frac{1}{2}\partial_\mu\sigma\partial^\mu\sigma + \frac{1}{2}m_\sigma^2\sigma^2 - U(\sigma) \\ & + \sum_l \bar{l}(-i\gamma^\mu\partial_\mu - m_l)l. \end{aligned}$$

Here,  $B$  are the Dirac spinors for baryons and  $\mathbf{t}$  is the isospin operator. The sums include baryons,  $B = n, p, \Lambda, \Sigma$  and  $\Xi$ , and leptons,  $l = e^-$  and  $\mu^-$ . The field strength tensors for the  $\omega$  and  $\rho$  mesons are  $W_{\mu\nu} = \partial_\mu\omega_\nu - \partial_\nu\omega_\mu$  and  $\mathbf{B}_{\mu\nu} = \partial_\mu\mathbf{b}_\nu - \partial_\nu\mathbf{b}_\mu$ , respectively. The potential  $U(\sigma)$  represents the self-interactions of the scalar field and is taken to be of the form

$$U(\sigma) = \frac{1}{3}bM_n(g_{\sigma N}\sigma)^3 + \frac{1}{4}c(g_{\sigma N}\sigma)^4. \quad (14)$$

Electrons and muons are included in the model as non-interacting particles, since their interactions give small contributions compared to those of their free Fermi gas parts.

In the mean field approximation, the baryon source currents and meson fields are replaced by their ground state expectation values  $\sigma_0, \omega_0$  and  $b_0$ . The resulting set of non-linear equations are solved for the meson fields and the particle fractions under the constraints of charge neutrality and  $\beta$ -equilibrium. At zero temperature, the particle fractions  $n_i \propto k_{Fi}^3$ . The general beta equilibrium condition

$$\mu_i = b_i\mu_n - q_i\mu_l, \quad (15)$$

where  $b_i$  is the baryon number of particle  $i$  and  $q_i$  is its charge, determines whether a particular baryon will be present at a given density. This will be the case if the lowest lying energy state of that baryon in matter, which is implicitly density dependent through the values of the meson fields, is less than its chemical potential as dictated by  $\beta$ -equilibrium. The value of  $k_{FB}$  is thus determined by the requirement that

$$\mu_B = e_B(k_{FB}) = g_{\omega B}\omega_0 + g_{\rho B}\mathbf{t}_3 b_0 + \sqrt{k_{FB}^2 + M_B^{*2}}, \quad (16)$$

where the Dirac effective mass  $M_B^* = M_B - g_{\sigma B}\sigma_0$ .

In the nucleon sector, the constants  $g_{\sigma N}, g_{\omega N}, g_{\rho N}, b$  and  $c$  are determined by reproducing the nuclear matter equilibrium density  $n_0 = 0.16 \text{ fm}^{-3}$ , and the binding energy per nucleon, the symmetry energy coefficient, the compression modulus, and the nucleon Dirac effective mass,  $M^*$ , at  $n_0$ . Numerical values of the coupling constants so chosen in different models are shown in Table 2. Models from Glendenning and Moszkowski (1991) are termed GM and models from Horowitz and Serot (1981) are termed HS. The different values shown reflect the prevalent uncertainty in the nuclear matter compression modulus and the effective mass  $M^*$ .

In the GM models, the hyperon coupling constants are determined by reproducing the binding energy of the  $\Lambda$  hyperon in nuclear matter. Parameterizing the hyperon-meson couplings in terms of nucleon-meson couplings through

$$x_{\sigma H} = g_{\sigma H}/g_{\sigma N}, \quad x_{\omega H} = g_{\omega H}/g_{\omega N}, \quad x_{\rho H} = g_{\rho H}/g_{\rho N}, \quad (17)$$

the  $\Lambda$  binding energy at nuclear density is given by  $(B/A)_\Lambda = -28 = x_{\omega\Lambda}g_{\omega N}\omega_0 - x_{\sigma\Lambda}g_{\sigma N}\sigma_0$ , in units of MeV. Thus, a particular choice of  $x_{\sigma\Lambda}$  determines  $x_{\omega\Lambda}$  uniquely. To keep the number of parameters small, the coupling constant ratios for all the different hyperons are assumed to be the same. That is

$$x_\sigma = x_{\sigma\Lambda} = x_{\sigma\Sigma} = x_{\sigma\Xi}, \quad (18)$$

TABLE 2  
NUCLEON-MESON COUPLING CONSTANTS

Model	$\frac{g_\sigma}{m_\sigma}$ (fm)	$\frac{g_\omega}{m_\omega}$ (fm)	$\frac{g_\rho}{m_\rho}$ (fm)	b	c	$\frac{M^*}{M}$
GM1	3.434	2.674	2.100	0.00295	-0.00107	0.70
GM2	3.025	2.195	2.189	0.00348	0.01328	0.78
GM3	3.151	2.195	2.189	0.00866	-0.00242	0.78
HS1,HS2,HS3	3.974	3.477	2.069	0.0	0.0	0.54

NOTE.— Constants from Glendenning and Moszkowski (1991) are termed GM and those from Horowitz and Serot (1981) are termed HS. HS models do not have scalar self-couplings which leads to effective masses which are significantly smaller than those of GM models.

TABLE 3  
RATIOS OF HYPERON-MESON TO NUCLEON-MESON COUPLING CONSTANTS

Model	$x_{\sigma\Lambda}$	$x_{\sigma\Sigma}$	$x_{\sigma\Xi}$	$x_{\omega\Lambda}$	$x_{\omega\Sigma}$	$x_{\omega\Xi}$	$x_{\rho\Lambda}$	$x_{\rho\Sigma}$	$x_{\rho\Xi}$
GM1	0.600	0.600	0.600	0.653	0.653	0.653	0.600	0.600	0.600
GM2,GM3	0.600	0.600	0.600	0.659	0.659	0.659	0.600	0.600	0.600
HS1	0.600	0.540	0.600	0.650	0.670	0.650	0.600	0.670	0.600
HS2	0.600	0.770	0.600	0.650	1.00	0.650	0.600	0.670	0.600
HS3	0.600	0.770	0.770	0.650	1.00	1.00	0.600	0.670	0.670

NOTE.—  $x_{iH} = g_{iH}/g_{iN}$ , where  $i = \sigma, \omega$  or  $\rho$  and  $H$  is a hyperon.

and similarly for the  $\omega$  and  $\rho$  mesons. Further,  $x_\rho$  is set equal to  $x_\sigma$ .

In a recent analysis of  $\Sigma^-$  atoms, Mareš et al. (1995) obtain reasonable fits with  $x_{\omega\Sigma} = 2/3$  and 1, and  $x_{\sigma\Sigma} = 0.54$  and 0.77 based on a mean field description of nuclear matter using the nucleon couplings of Horowitz & Serot (1981). Lacking further inputs from data, Mareš et al. assume that the couplings of the  $\Sigma$  and  $\Xi$  are equal to those of the  $\Lambda$  hyperon. This set of couplings are termed HS1 in Table 3. Following Knorren, Prakash & Ellis (1995), we have relaxed the above assumption about the couplings of the  $\Sigma$  and  $\Xi$  in parameter sets HS2 and HS3 to explore the sensitivity of the thresholds to small changes in the couplings.

In Figure 1, we show the relative fractions of the baryons and leptons in charge neutral and  $\beta$ -equilibrated matter. For the GM models, the  $\Sigma^-$  hyperon appears at a density lower than the  $\Lambda$  hyperon. This is because the somewhat higher mass of the  $\Sigma^-$  is compensated by the presence of the  $e^-$  chemical potential in the equilibrium condition of the  $\Sigma^-$ . More massive and more positively charged particles appear at higher densities. With the appearance of the negatively charged  $\Sigma^-$ , which competes with leptons in maintaining charge neutrality, the lepton concentrations begin to fall. The important point is that, with increasing density, the system contains many baryon species with nearly equal concentrations.

The relative concentrations of the baryons in the HS1 model are qualitatively similar to

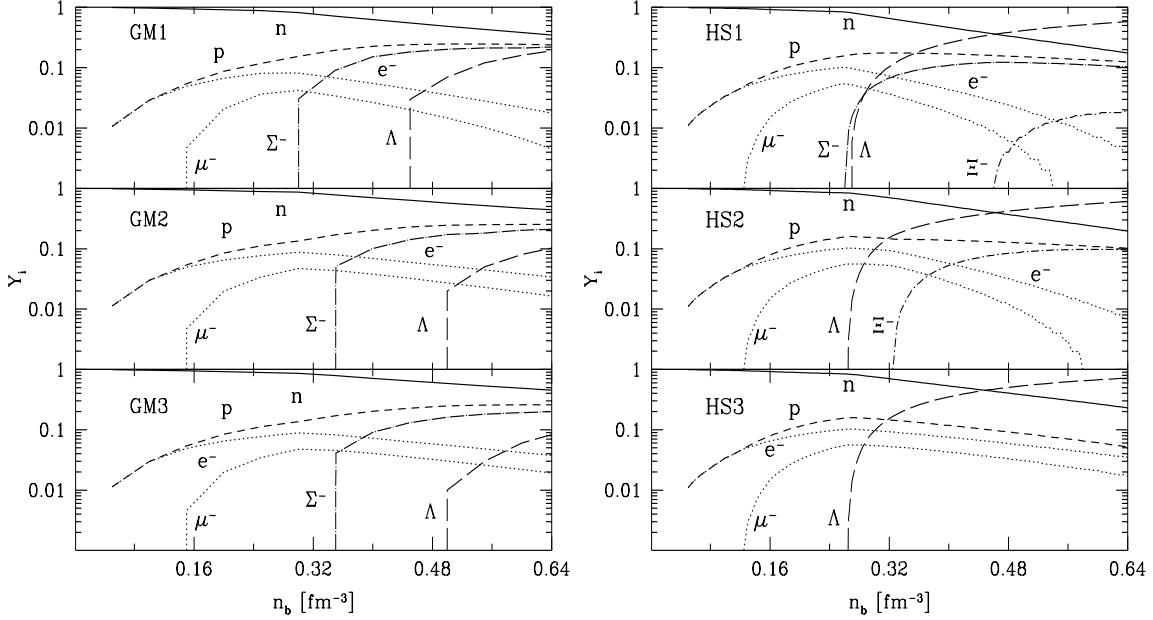


Figure 1: Particle fractions,  $Y_i = n_i/n_b$ , for the models shown in Table 3.

those of the GM models, although substantial quantitative differences exist. Note, however, that relaxing the assumption about the  $\Sigma$  and  $\Xi$  couplings has large effects on the appearance of negatively charged particles, as seen from the results of models HS2 and HS3. Increasing the coupling constants of a hyperon species delays its appearance to a higher density. This is because the threshold equation, Eq. (16), receives contributions from the  $\sigma$ ,  $\omega$  and  $\rho$  fields, the net result being positive due to that of the  $\omega$ . If all the couplings are scaled up, the positive contribution becomes larger, and hence the appearance of the particle is delayed to a higher density. The  $\Sigma$  couplings of set HS2 are larger than those of set HS1, so the  $\Sigma^-$  no longer appears, thus allowing the chemical potential  $\mu$  to continue rising. This allows the  $\Xi^-$  to appear at  $n/n_0 \cong 2.2$ , essentially substituting for the  $\Sigma^-$ . Were we to reduce the  $\Xi$  couplings on the grounds that this hyperon contains two strange quarks, the  $\Xi^-$  would appear at an even lower density. In model HS3, both the  $\Sigma$  and  $\Xi$  couplings are increased. Neither of them now appear, leaving the  $\Lambda$  as the only strange particle in matter. Clearly, the thresholds for the strange particles are sensitive to the coupling constants, which are presently poorly constrained by either theory or experiment. Notwithstanding these caveats, it is clear that one or the other hyperon species is likely to exist in dense matter.

As we will see later, the effective masses of the baryons play an important role in determining the differential cross sections. Figure 2 shows the density dependence of the nucleon effective mass, which shows significant differences between models with scalar self-interactions (GM) and those without (HS). Scalar self-interactions, which lead to low  $\sigma N$  couplings in GM models, result in  $M^*$ s which are larger than those of the HS models, in

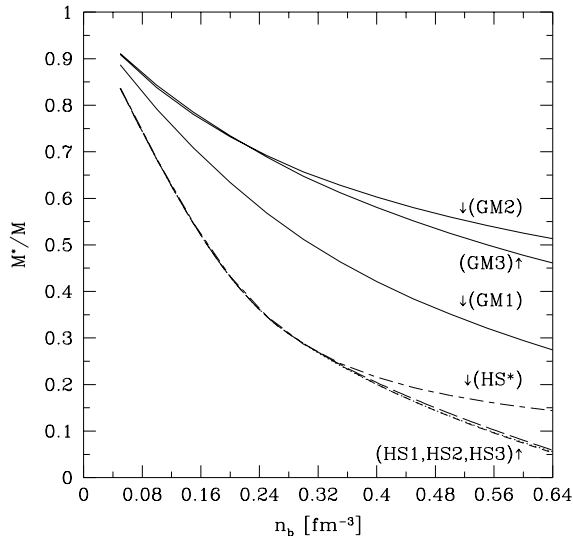


Figure 2: Nucleon effective mass  $M^*$  for the models discussed in the text. The plot labelled HS\* is for matter containing nucleons and leptons only, with couplings of model HS.

which  $M^*$  falls rapidly, due to a relatively large  $\sigma N$  coupling. The presence of hyperons further hastens this fall off with density, which is evident from the density dependence of  $M^*$  in matter with nucleons and leptons only (see the curve labeled HS\*). The behavior of the effective masses tending to zero at a finite baryon density is generic to models with hyperons, as shown by Knorren, Prakash & Ellis (1995). Whether this feature may be interpreted as strangeness-induced chiral restoration depends on whether the effective mass can be viewed as an order parameter. In the context of neutrino interactions, which is our main interest here, the results of Figure 2 may be taken to encompass the current uncertainty in the knowledge of strong interactions.

## 4 Results and Discussion

Since the neutrino coupling is species specific (see Table 1), the response of a multi-component system will depend on the relative abundance of the various particles. Pauli blocking, which plays an important role at zero temperature, restricts the neutrinos to couple with particles lying close to their respective Fermi surfaces. The Fermi momenta and the effective masses of the various particles in different models are given in Table 4. Results here are for  $n_b = 0.4 \text{ fm}^{-3}$ .

Figure 3 shows the response function  $R_1$  at a density  $n_b = 0.4 \text{ fm}^{-3}$ . Models HS\* and GM3\* in the left panels are for matter with nucleons and leptons, while models HS3 and GM3 in the right panels include hyperons. For a given three-momentum transfer  $|q|$ , each particle species provides support to the response functions in the region  $0 \leq \omega \leq \omega_{max}$ ,

TABLE 4  
FERMI MOMENTA AND EFFECTIVE MASSES

Model	$n_b$ $fm^{-3}$	$k_{Fn}$ MeV	$k_{Fp}$ MeV	$k_{F\Sigma^-}$ MeV	$k_{F\Lambda}$ MeV	$k_{Fe^-}$ MeV	$k_{F\mu^-}$ MeV	$M_n^*$ MeV	$M_\Sigma^*$ MeV	$M_\Lambda^*$ MeV
GM1	0.4	385.2	274.2	236.3	0.0	171.1	134.3	395.4	867.4	790.5
GM3	0.4	401.0	263.9	201.1	0.0	187.2	154.3	545.4	957.4	880.5
HS1	0.4	348.4	249.0	214.3	286.5	158.2	117.7	188.1	788.1	666.1
HS3	0.4	364.4	220.4	0.0	317.2	189.6	157.4	191.8	618.4	668.3

NOTE.— Results are for  $n_b = 0.4 \text{ fm}^{-3}$ .

where  $\omega_{max}$  for particle-hole excitations is determined by energy-momentum conservation:

$$\omega_{max} = \sqrt{E_{Fi}^{*2} + q^2 + 2k_{Fi}|q|} - E_{Fi}^*,$$

where  $E_{Fi}^* = \sqrt{k_{Fi}^2 + M_i^{*2}}$ . For  $M_i^* \gg k_{Fi}$ , this reduces to the non-relativistic condition  $\omega_{max} = (k_{Fi}/M_i^*)|q|$ . The response functions for electron and muon scattering extend up to  $\omega \cong |q|$ . Similar behavior is exhibited by the response functions of baryons at high density as they become increasingly relativistic. In models HS\* and HS3, the neutrons and protons are moderately relativistic, due to their relatively small effective masses, which leads to flatter and wider responses, in contrast to the results for models GM3 and GM3\*, where relativistic effects are important only for the leptons. For  $\omega/\omega_{max} \ll 1$ , the response functions are linear with slopes proportional to  $E_{Fi}^*/|q|$ . For non-relativistic particles, the response is linear up to  $\omega = \omega_{max}$ , with a sharp kinematical cut-off thereafter. For relativistic particles, the response quickly becomes non-linear with  $\omega$  and exhibits a maximum at  $\omega$  somewhat less than  $\omega_{max}$ .

The bulk of the response is provided by the baryons. At  $n_b = 0.4 \text{ fm}^{-3}$ , model HS3 predicts only the  $\Lambda$  hyperon to be present and that the  $n$  and  $\Lambda$  abundance are nearly the same. However, at tree level, neutrinos do not couple to the  $\Lambda$ , and thus the bulk of the response is from the neutrons. In contrast, model GM3 allows only the  $\Sigma^-$  hyperon to be present (up to  $n_b = 0.4 \text{ fm}^{-3}$ ), to which neutrinos couple. Since  $M_{\Sigma^-}^* > M_n^*$ , the  $\Sigma^-$  response is larger than that of the neutron for  $\omega$  less than the  $\omega_{max}$  of the  $\Sigma^-$ . These results clearly show that the response is sensitive to both the charge and the abundance of strangeness-bearing components in matter. Further, the response of matter containing strange baryons differs (right panels) significantly from that of matter with nucleons only (left panels).

In Figure 4, we show the differential cross sections per unit volume from Eq. (3), for  $\nu_e$  scattering in the different models shown in Table 4, and, for  $n_b = 0.4 \text{ fm}^{-3}$ . The results, which receive contributions from all three response functions in Eqs. (12) through (13), highlight the role of the composition and of the effective mass  $M^*$ , both of which vary between the different models. The structure in these cross sections may be easily understood in terms of the various baryonic components present. For example, in models GM1 and HS1, the particles present are  $(\Sigma^-, p, n)$  and  $(\Sigma^-, p, \Lambda, n)$ , respectively, in increasing order

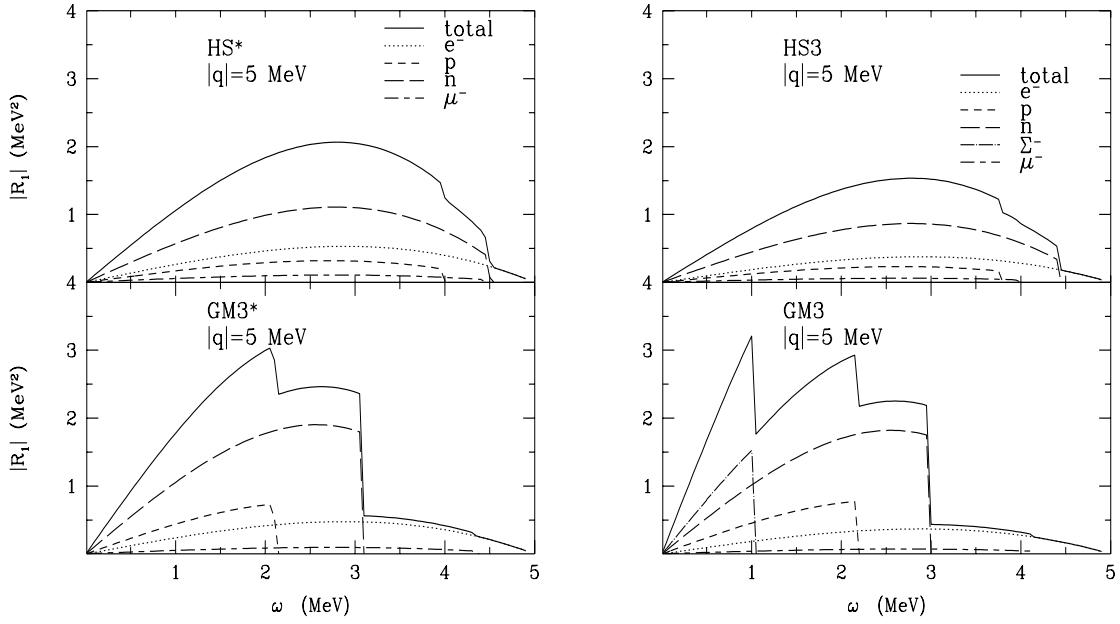


Figure 3: -Response function  $R_1$  from Eq. (12), as a function of the energy transfer  $\omega$  for  $n_b = 0.4 \text{ fm}^{-3}$ . Models HS\* and GM3\* in the left panels are for matter with nucleons and leptons only, while models HS3 and GM3 in the right panels include hyperons.

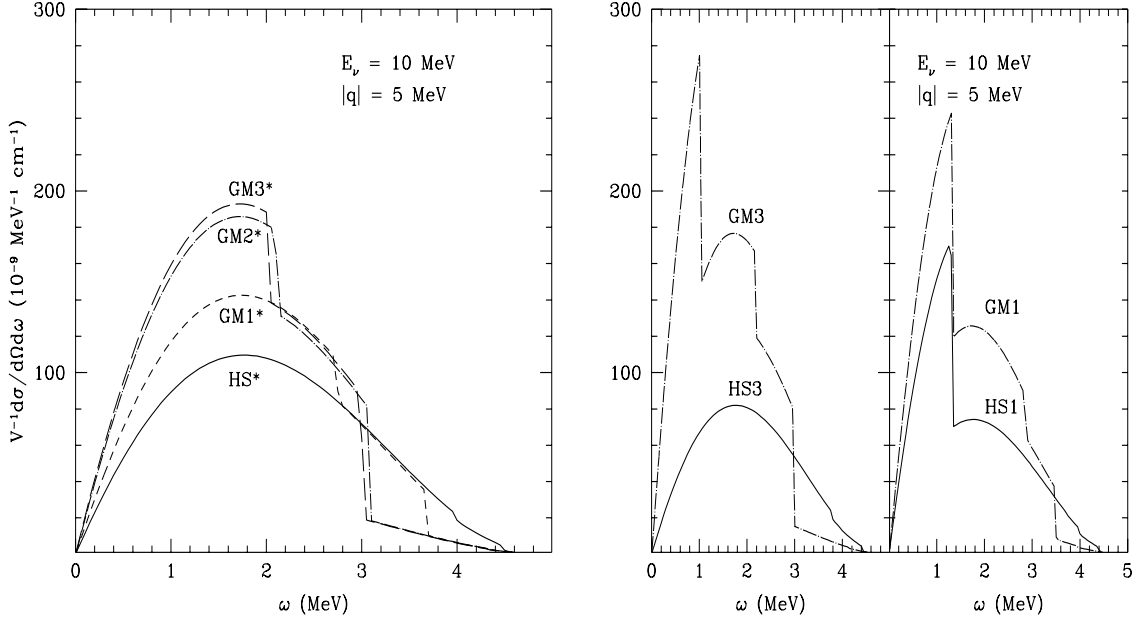


Figure 4: Differential cross sections from Eq. (3), at  $n_b = 0.4 \text{ fm}^{-3}$ . In all models except HS3, the contribution from the  $\Sigma^-$  hyperon is clearly seen in the low energy transfer region. Model designations are the same as in Figure 3.

of  $k_{Fi}$ . In contrast, for models GM3 and HS3, we have  $(\Sigma^-, p, n)$  and  $(p, \Lambda, n)$ , respectively. The  $\Sigma^-$ , when present, enhances the cross sections for  $\omega < 1$  MeV. The signature of the different effective masses in the various models is evident both from the magnitudes and the shapes of the differential cross sections.

A qualitative understanding of the differential cross sections may be obtained by considering the non-relativistic approximation for the baryon polarization  $\Pi^{\alpha\beta}$ . In this limit, only  $\text{Im } \Pi^{00}$  contributes, giving

$$\frac{1}{V} \frac{d^3\sigma}{d\Omega^2 dE'_\nu} = \frac{G^2}{4\pi^3} \frac{E'_\nu}{E_\nu} |q|^2 A \sum_i [C_{Vi}^2 S(q, \omega) + 3C_{Ai}^2 \mathcal{S}(q, \omega)], \quad (19)$$

where  $S(q, \omega)$  is the scalar density response function and  $\mathcal{S}(q, \omega)$  is the spin density response function. This result has been obtained earlier by Iwamoto & Pethick (1982). In the non-relativistic limit,  $S(q, \omega) = \mathcal{S}(q, \omega)$  in the mean field models, since there are no explicit spin-dependent interactions. For small energy transfers,

$$S(q, \omega) = \frac{M_i^{*2}}{2\pi|q|} \omega, \quad \text{for } 0 \leq \omega \leq \frac{k_f}{M^*} |q|.$$

Thus, at low density, when  $M_i^* \gg k_{Fi}$ , the magnitude of the differential cross sections is essentially determined by the effective mass. Note, however, that the total cross section does

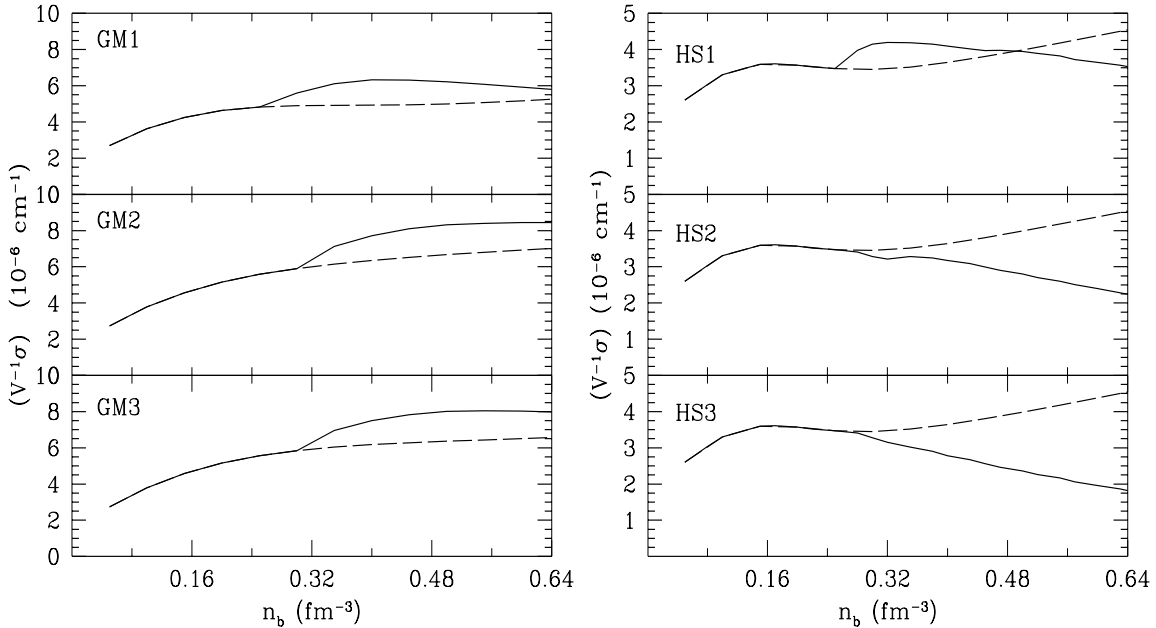


Figure 5: The total cross section per unit volume for 10 MeV electron neutrinos for the models discussed in §2. Solid lines show results with hyperons and dashed lines show results with nucleons only.

not depend on  $M^*$  in this limit, since  $S(q, \omega)$  depends linearly on  $\omega$  and the kinematical cutoff on  $\omega$  is inversely proportional to  $M^*$ . This is in accordance with the sum rule for density-density fluctuations in the non-relativistic limit.

The total cross section per unit volume is evaluated by integrating Eq. (9) over the kinematically allowed region. At zero temperature, only  $\omega \geq 0$  contributes, due to Pauli blocking and  $\omega \leq |q| \leq (2E_\nu - \omega)$ , where  $E_\nu$  is the incident neutrino energy. The density dependence of the cross sections is shown in Figure 5. The appearance of the  $\Sigma^-$  increases the cross section relative to that in matter without the  $\Sigma^-$ . However, the appearance of the  $\Lambda$ , which furnishes baryon number, results in a decrease of the cross section, since the neutron abundance is decreased. At high density, when the baryons become increasingly relativistic, the total cross sections begin to show sensitivity to  $M_i^*$ , unlike in the non-relativistic limit, where such a dependence is absent. This partly accounts for the differences in the cross sections between the various models.

Note also the large suppression (almost a factor of 2 at high density) in the cross sections for models without scalar self-coupling (HS) compared to those with such couplings (GM).

The results in Figure 5 give inverse collision mean free paths of 10 MeV neutrinos interacting via neutral current reactions. The transport and energy degradation mean free paths are, in general, different from the collision mean free path. The former involve appropriate  $q$  or  $\omega$  weighted integrals of the differential cross sections. However, for neutrino diffusion, the collision mean free path is expected to be similar in magnitude to the transport mean free paths (Goodwin & Pethick 1982).

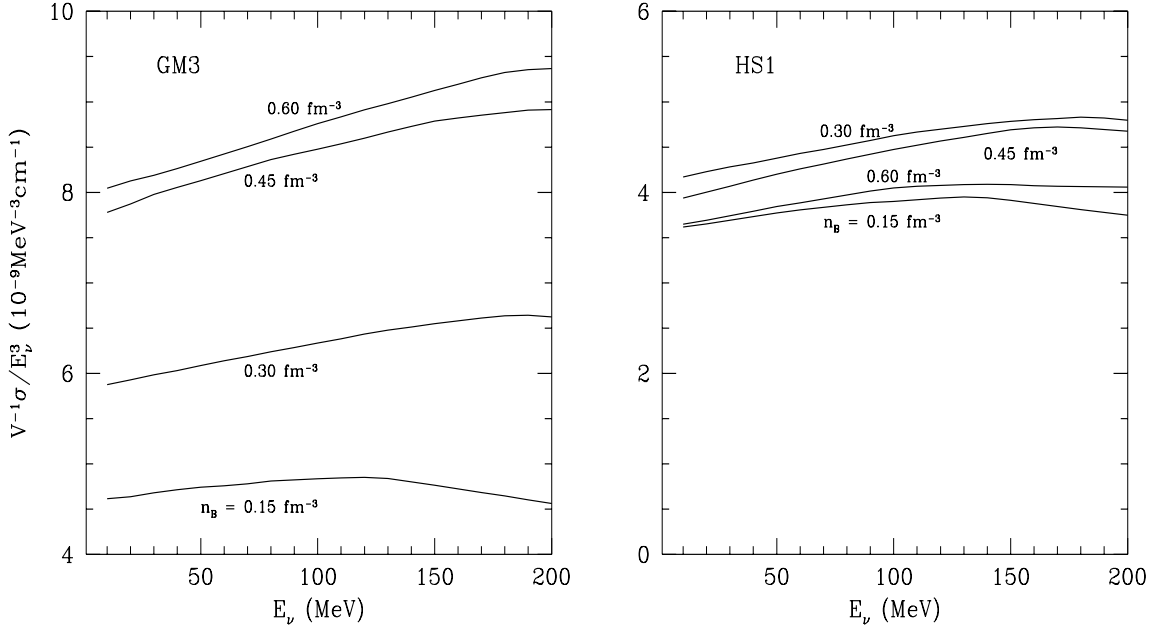


Figure 6: Energy dependence of the scaled (with  $E_\nu^3$ ) total cross section per unit volume as a function of neutrino energy  $E_\nu$ .

Figure 6 shows the energy dependence of the cross sections, scaled by  $E_\nu^3$ , for different baryon densities. As expected for zero temperature matter, the cross sections in both cases vary essentially as  $E_\nu^2 \cdot E_\nu$ , where the first factor arises from the basic neutrino cross section on a single baryon and the second factor arises from the number of participating particles of a given species. Note, however, that at high density, the baryon number density dependence is non-monotonic for the model HS1. This may be understood in terms of the rapidly decreasing effective masses in this case.

It is worthwhile to mention that, in a nuclear medium, the effective value of  $|C_A|$  is quenched (Wilkinson 1973; Rho 1974). At the nuclear equilibrium density  $n_0 = 0.16 \text{ fm}^{-3}$ ,  $|C_A| \simeq 1$ , and it is expected to remain at approximately this value for densities not too far above  $n_0$ . Modifications of this nature require that the calculations be carried out beyond the mean field level for the strongly interacting particles. A first orientation of such effects may, however, be obtained by using  $C_A = 1$  in the case of nucleons-only matter in the present calculations. In this case, the cross sections are reduced by about (15-20)%. At present, however, it is not known if the presence of hyperons at  $n_b \gg (2-3)n_0$  brings about additional modifications of  $|C_A|$ .

## 5 Conclusions

Many calculations of the composition of dense matter indicate that strangeness-rich matter should be present in the core of neutron stars. In this work, we have identified neutral current neutrino interactions with hyperons that are important sources of opacity. We find that significant contribution to the neutrino opacity arises from scattering involving  $\Sigma^-$  hyperons. Although the lowest order tree level contributions from the neutral  $\Lambda$  and  $\Sigma^0$  vanish, these particles, when present, furnish baryon number which decreases the relative concentrations of nucleons. This leads to significant reductions in opacity.

The neutrino cross section depends sensitively on the Fermi momenta and effective masses of the various particles present in matter. Whether or not a particular hyperon is present depends on the many-body description of charge neutral beta-equilibrated matter. We find that as long as one or the other hyperon is present, the cross sections are significantly modified from the case of nucleons-only matter. Strong interactions of strange particles in matter is currently poorly known, our knowledge being restricted to regions near nuclear equilibrium density. In field theoretical descriptions of dense matter, relatively small changes in the hyperon couplings lead to large differences in the composition and the effective masses of the various particles. This emphasizes the need to pin down the mass shifts of baryons in dense matter, particularly at high density (for initial attempts, see, for example, Savage & Wise 1995). In this work, we have explored the extent to which the cross sections are modified due to the prevalent uncertainty in strong interactions. Depending on the behavior of the effective masses at high density, the opacities may vary by a factor of about 2 at high density.

Our findings here suggest several directions for further study. The extension of these calculations to finite temperature and to include correlations between the different particles is straightforward and is under progress. During its early evolution, the protoneutron star attains entropies per baryon of order 1-2 and central temperatures of order 30-50 MeV. Such matter is degenerate, since the chemical potentials of the constituents are typically of order 200-300 MeV (Prakash et al. 1995). Hence, the zero temperature results are not expected to be greatly modified. The presence of charged particles, such as the  $\Sigma^-$ , could make available low energy collective plasma modes through electromagnetic correlations, in addition to the scalar, vector and iso-vector correlations. Effects of strangeness on lepton number and energy transport may be studied by employing energy averages (Rosseland means) of the opacities in present protoneutron codes. Tables of such useful average opacities will be made generally available. With new generation neutrino detectors capable of recording thousands of neutrino events, it may be possible to distinguish between different scenarios observationally.

This work was supported in partly the U.S. Department of Energy under contract number DOE/DE-FG02-88ER-40388 and by the NASA grant NAG 52863. We thank Jim Lattimer and Chuck Horowitz for helpful discussions.

## References

Bionta, R. M., et al., 1987, Phys. Rev. Lett. 58, 1494

Bruenn, S., 1985, ApJ. Suppl. 58, 771  
 Burrows, A., 1988, ApJ 334, 891  
 —, 1990, Ann. Rev. Nucl. Sci. 40, 181  
 Burrows, A & Lattimer, J. M., 1986, ApJ 307, 178  
 Burrows, A & Mazurek, T. J., 1982, ApJ 259, 330  
 Cooperstein, J., 1988, Phys. Rep. 163, 95  
 Ellis, J., Kapusta, J. I., & Olive, K. A. 1991, Nucl. Phys. B348, 345  
 Ellis, P. J., Knorren, R., & Prakash, M., 1995, Phys. Lett. B349, 11  
 Gaillard, J.-M., & Sauvage, G. 1984, Ann. Rev. Nucl. Part. Sci., 34, 351  
 Glendenning, N. K., & Moszkowski, S. A. 1991, Phys. Rev. Lett. 67, 2414  
 Goodwin, B. T., 1982, ApJ 261, 321  
 Goodwin, B. T. & Pethick, C. J. 1982, ApJ 253, 816  
 Hirata, K., et al., 1987, Phys. Rev. Lett. 58, 1490  
 Horowitz, C. J., 1992, Phys. Rev. Lett. 69, 2627  
 Horowitz, C. J., & Serot, H. S. 1981, Nucl. Phys. A368, 503  
 Horowitz, C. J., & Wehrberger, K., 1991a, Nucl. Phys. A531, 665  
 —, 1991b, Phys. Rev. Lett. 66, 272  
 —, 1992, Phys. Lett. B226, 236  
 Iwamoto, N. 1982, Ann. Phys. 141, 1  
 Iwamoto, N., & Pethick, C. J., 1982, Phys. Rev. D25, 313  
 Kaplan, D. B., & Nelson, A. E. 1986, Phys. Lett. B175, 57  
 —, 1986, Phys. Lett. B179, 409 (E)  
 Kapusta, J. A., & Olive, K. A., 1990, Phys. Rev. Lett. 64, 13  
 Keil, W., & Janka, H. T., 1995, Astron. & Astrophys. 296, 145  
 Knorren, R., Prakash, M., & Ellis, P. J., 1995, Phys. Rev. C52, 3470  
 Lamb, D. Q., 1978, Phys. Rev. Lett. 41, 1623  
 Lamb, D. Q., & Pethick, C. J., 1976, ApJ 209, L77  
 Mareš, J., Friedman, E., Gal. A., & Jennings, B. K., 1995, preprint nucl-th/9505003  
 Maxwell, O., 1987, ApJ 316, 691  
 Mazurek, T. J., 1975, Astrophys. Space. Sci. 35, 117  
 Prakash, M., Prakash, Manju, Lattimer, J. M., & Pethick, C. J. 1992, ApJ 390, L77  
 Prakash, M., Cooke, J., & Lattimer, J. M., 1995, Phys. Rev. D52, 661  
 Prakash, M., Bombaci, I., Prakash, Manju, Ellis, P. J.,  
 Lattimer, & J. M., & Knorren, R., 1995, Phys. Rep., To be submitted  
 Reddy, S., and Prakash, M., 1995, Proc. of the 11th Winter Workshop on Nuclear  
 Dynamics, Key West, Fl, Feb 11–18, 1995  
 Rho., M. 1974, Nucl. Phys. A231, 493. Sato, K., 1975, Prog. Theor. Phys. 53, 595  
 Savage, M., & Wise, M., 1995, Phys. Rev. D, in press  
 Sawyer, R. F., 1975, Phys. Rev. D11, 2740  
 —, 1989, Phys. Rev. C40, 865  
 —, 1995, Phys. Rev. Lett. C75, 2260  
 Sawyer, R. F. & Soni, R., 1979, ApJ 230, 859  
 ed. J. W. Negele & E. Vogt (New York: Plenum)  
 Serot, B. D., & Walecka, J. D., 1986, in Adv. Nucl. Phys. 16,  
 Thorsson, V., Prakash, M., & Lattimer, J. M. 1994, Nucl. Phys. A572, 693

Tubbs, D. L., & Schramm, D. N., 1975, ApJ 201, 467  
van den Horn. L. J., & Cooperstein, J., 1986, ApJ 300, 142  
Wilkinson, D. H., 1973, Phys. Rev. C7, 930.